Signal to background interference in $pp \to tH^- \to tW^- b\bar{b}$ at the LHC Run II

Abdesslam Arhrib,[1] Rachid Benbrik,[2,3,4] Stefano Moretti,[5] Rui Santos,[6,7,8] and Pankaj Sharma[9]

[1]*Faculté des Sciences et Techniques, Abdelmalek Essaadi University, B.P. 416 Tangier, Morocco*
[2]*LPHEA Faculté Semlalia Marrakech and MSISM Team, Faculté Polydisciplinaire de Safi,*
Sidi Bouzid, BP 4162 Safi, Morocco
[3]*School of Physics Sciences, University of Chinese Academy of Sciences, Beijing 100039, China*
[4]*Center for future high energy physics, Chinese Academy of Sciences, Beijing 100039, China*
[5]*School of Physics and Astronomy, University of Southampton,*
Southampton SO17 1BJ, United Kingdom
[6]*ISEL—Instituto Superior de Engenharia de Lisboa, Instituto Politécnico de Lisboa,*
1959-007 Lisboa, Portugal
[7]*Centro de Física Teórica e Computacional, Faculdade de Ciências, Universidade de Lisboa,*
Campo Grande, Edifício C8, 1749-016 Lisboa, Portugal
[8]*LIP, Departamento de Física, Universidade do Minho, 4710-057 Braga, Portugal*
[9]*ARC Center of Excellence for Particle Physics at the Terascale, Department of Physics,*
University of Adelaide, 5005 Adelaide, South Australia

We investigate in the Large Hadron Collider (LHC) environment the possibility that sizeable interference effects between a heavy charged Higgs boson signal produced via $bg \to tH^-$ (+c.c.) scattering and decaying via $H^- \to W^- A \to W^- b\bar{b}$ (+c.c.) and the irreducible background given by $bg \to tW^- b\bar{b}$ topologies could spoil current search approaches where the former and latter channels are treated separately. The rationale for this comes from the fact that a heavy charged Higgs state can have a large width, which can also happen for the CP-odd neutral Higgs state emerging in the ensuing decays, which in turn enables such interferences. We conclude that effects are very significant, both at the inclusive and exclusive level (i.e., both before and after $H^\pm$ selection cuts are enforced, respectively) and typically of a destructive nature. This, therefore, implies that currently established LHC reaches for heavy charged Higgs bosons require some level of rescaling. However, this is possible *a posteriori*, as the aforementioned $H^\pm$ selection cuts shape the interference contributions at the differential level in a way similar to that of the isolated $H^\pm$ signal, so there is no need to reassess the efficiency of the individual cuts. We show such effects quantitatively by borrowing benchmark points from different Yukawa types of a 2-Higgs doublet model parameter space for $H^\pm$ values starting from around 200 GeV.

I. INTRODUCTION

As much as one would welcome the production of a light charged Higgs boson from top-quark decay at the LHC, as the event rate would be plentiful, it must be recognized by now that the likelihood of this being a design of nature is becoming slimmer and slimmer. This is because extensive searches have been carried out by the ATLAS and CMS Collaborations in this mode, assuming a variety of $H^\pm$ decay channels, none of which has been fruitful. Hence, it is becoming more likely that if such a state indeed exists in nature, it will be heavier than the top quark, i.e., $M_{H^\pm} > m_t$.[1]

The call for establishing an $H^\pm$ signal comes from an intriguing theoretical consideration—that the discovery of a (singly) charged Higgs boson would signal the existence of a second Higgs doublet in addition to the standard model (SM)-like one already established through the discovery of

---

[1]We should note, however, that both the production and decay modes used in all present searches may have a strong dependence on the parameters of the model. In particular, versions of the 2-Higgs Doublet Model (2HDM) [1], for example, a very large value of the parameter $\tan\beta$, the ratio of the vacuum expectation values (VEVs) of the two doublets, will render useless any search involving Yukawa couplings. For these scenarios only processes involving the electromagnetic coupling of the charged Higgs would be able to settle the issue of existence of light charged Higgs bosons.

the $W^{\pm}$ and Z bosons at the $Sp\bar{p}S$ [2,3] in the 1980s and of a Higgs boson itself at the LHC only five years ago [4,5]. Such a spinless field can naturally be accommodated in 2HDMs, which are the standard theoretical frameworks assumed in experimental analyses. Indeed, in their CP-conserving versions, 2HDMs present in their spectra, after spontaneous electroweak symmetry breaking (EWSB), five physical Higgs states: the neutral pseudo-scalar (A), the lightest (h) and heaviest (H) neutral scalars, and two charged ones ($H^{\pm}$).

Of all 2HDM Yukawa types (see [6] for a review), we concentrate here on the 2HDM type II, flipped, and type III ones (to be defined later). This is because such Yukawa types of 2HDMs have a preference for heavy charged Higgs bosons. In the 2HDM type II and flipped, constraints from $b \to s\gamma$ decays put a lower limit on the $H^{\pm}$ mass at about 580 GeV, rather independently of $\tan\beta$ [7,8]. In the 2HDM type III, such constraint is relaxed, yet the combination of all available experimental data places a lower limit on $M_{H^{\pm}}$ at about 200 GeV or possibly even less [9]. Hence, both such 2HDM scenarios provide parameter spaces that are suitable to benchmark experimental searches for heavy charged Higgs bosons.

Such a heavy mass region is very difficult to access because of the large reducible and irreducible backgrounds associated with the main decay mode $H^+ \to t\bar{b}$, following the dominant production channel $bg \to tH^-$ [10]. (Notice that the production rate of the latter exceeds by far that of other possible production modes, like those identified in [1,11–13], thus rendering it the only accessible production channel at the CERN machine in the heavy mass region.) The analysis of the $H^+ \to t\bar{b}$ signature has been the subject of many early phenomenological studies [14–17], their conclusion being that the LHC discovery potential might be satisfactory, so long that $\tan\beta$ is small (≤ 1.5) or large (≥ 30) enough and the charged Higgs boson mass is below 600 GeV or so. Such rather positive prospects have recently been revived by an ATLAS analysis of the full Run-I sample [18], which searched precisely for the aforementioned $H^{\pm}$ production and decay modes, by exploring the mass interval from 300 to 600 GeV. In fact, an excess with respect to the SM predictions was observed for $M_{H^{\pm}}$ hypotheses in the heavy mass region. While CMS does not confirm such an excess [19], the increased sensitivity that the two experiments are accruing with current Run-II data calls for a renewed interest in the search for such elusive Higgs states.

In this spirit, and recognizing that the $H^+ \to t\bar{b}$ decay channel eventually produces a $W^+b\bar{b}$ signature, Ref. [20] attempted to extend the reach afforded by this channel by exploiting the companion signature $H^+ \to h_{\rm SM}W^+ \to b\bar{b}W^+$, where $h_{\rm SM}$ is the SM-like Higgs boson discovered at CERN in 2012 (which is either the h or H state of 2HDMs). The knowledge of its mass now provides in fact an additional handle in the kinematic analysis when reconstructing a Breit-Wigner resonance in the $h_{\rm SM} \to b\bar{b}$ decay channel, thereby significantly improving the signal-to-background ratio afforded by pre-Higgs-discovery analyses [21,22]. Such a study found that significant portions of the parameter spaces of several 2HDMs are testable at Run II.

Spurred by the aforementioned experimental results and building upon Ref. [20], some of us studied in Ref. [23] all intermediate decay channels of a heavy $H^{\pm}$ state also yielding a $W^{\pm}b\bar{b}$ signature, i.e., $H^+ \to t\bar{b}$, $hW^{\pm}$, $HW^{\pm}$ and $AW^{\pm}$, starting from the production mode $bg \to tH^-$ (+c.c.) (see also [24]). In doing so, we also took into account interference effects between these four channels, in the calculation of the total $H^{\pm}$ width as well as of the total yield in the cumulative $W^{\pm}b\bar{b}$ final state (wherein the $W^{\pm}$ decays leptonically), with the aim of maximizing the experimental sensitivity of ATLAS and CMS. The outcome of this analysis was that somewhat more inclusive search strategies (historically geared towards extracting the prevalent $H^+ \to t\bar{b}$ signature) ought to be deployed, that also capture $H^+ \to W^+ {\rm Higgs} \to W^+b\bar{b}$ channels. The exercise was performed specifically for a 2HDM type II, but results therein can easily be extrapolated to other Yukawa types.

In [23], only interferences between the four 2HDM channels yielding $H^+ \to W^+b\bar{b}$ decays were taken into account though, i.e., those between the different signal modes. While clearly all of these decay rates cannot be large at the same time, the important role of interferences amongst these decay modes was clearly established. However, in that analysis, the role of interference effects between any of these signals and the irreducible background was not discussed, as illustrative examples of the $H^{\pm}$ production and decay phenomenology were chosen so as to nullify their impact. Unfortunately, this condition can only be realized in specific regions of the 2HDM parameter space considered, whichever the Yukawa type, not everywhere. It is the purpose of this paper to address this issue, i.e., to assess the impact of interference effects between signal and irreducible background in the $H^+ \to W^+b\bar{b}$ channel on current phenomenological approaches to extract the latter. We will show that such effects are indeed very large for heavy $H^{\pm}$ masses over certain region of the 2HDM parameter space considered, both at the inclusive and exclusive level, i.e., before and after a selection is enforced, respectively. We will give some quantitative examples of this for the case of the specific $H^+ \to W^+A \to W^+b\bar{b}$ signal mode in three different Yukawa types of 2HDM (namely type II, flipped, and type III), for several $M_{H^{\pm}}$ choices.

The plan of this paper is as follows. In the next section, we introduce the 2HDM types considered and define their available parameter spaces based on current experimental and theoretical constraints in the following one. Then we proceed to describe what are the relevant diagrams entering

both signal and (irreducible) background as well as illustrate how we computed these. Section V is our numerical signal-to-background analysis. Finally, we draw our conclusions based on the results obtained in the last section of the paper.

II. THEORETICAL FRAMEWORK OF 2HDMS

In this section, we define the scalar potential and the Yukawa sector of the 2HDM type II, flipped, and type III. The most general scalar potential which is $SU(2)_L \otimes U(1)_Y$ invariant is given by [6,25]

$$
\begin{aligned}
V(\Phi_1, \Phi_2) \\
= m_1^2 \Phi_1^\dagger \Phi_1 + m_2^2 \Phi_2^\dagger \Phi_2 - (m_{12}^2 \Phi_1^\dagger \Phi_2 + \text{H.c.}) + \frac{1}{2} \lambda_1 (\Phi_1^\dagger \Phi_1)^2 \\
+ \frac{1}{2} \lambda_2 (\Phi_2^\dagger \Phi_2)^2 + \lambda_3 (\Phi_1^\dagger \Phi_1)(\Phi_2^\dagger \Phi_2) + \lambda_4 (\Phi_1^\dagger \Phi_2)(\Phi_1^\dagger \Phi_2) \\
+ \left[\frac{\lambda_5}{2} (\Phi_1^\dagger \Phi_2)^2 + (\lambda_6 \Phi_1^\dagger \Phi_1 + \lambda_7 \Phi_2^\dagger \Phi_2) \Phi_1^\dagger \Phi_2 + \text{H.c.} \right].
\end{aligned}
$$

(1)

The scalar doublets Φ_i ($i = 1, 2$) can be parametrized as

$$
\Phi_i(x) = \begin{pmatrix} \phi_i^+(x) \\ \frac{1}{\sqrt{2}} [v_i + \rho_1(x) + i\eta_1(x)] \end{pmatrix},
$$

(2)

with $v_{1,2} \geq 0$ being the VEVs satisfying $v = \sqrt{v_1^2 + v_2^2}$, with $v = 246.22$ GeV [26]. Hermiticity of the potential forces $\lambda_{1,2,3,4}$ to be real while $\lambda_{5,6,7}$ and m_{12}^2 can be complex. In this work, we choose to work in a CP-conserving potential where both VEVs are real and $\lambda_{5,6,7}$ and m_{12}^2 are also real.

After EWSB, three of the eight degrees of freedom in 2HDMs are the Goldstone bosons ($G^\pm$, G^0) and the remaining five degrees of freedom become the aforementioned physical Higgs bosons. After using the minimization conditions for the potential together with the $W^\pm$ boson mass requirement, we end up with nine independent parameters which will be taken as

$$
\{ m_h, m_H, m_A, m_{H^\pm}, \alpha, \beta, m_{12}^2, \lambda_6, \lambda_7 \},
$$

(3)

where $\tan \beta \equiv v_2/v_1$ and β is also the angle that diagonalizes the mass matrices of both the CP-odd and charged Higgs sector while the angle α does so in the CP-even Higgs sector.

The most commonly used version of a CP-conserving 2HDM is the one where the terms proportional to λ_6 and λ_7 are absent. This can be achieved by imposing a discrete Z_2 symmetry on the model that usually takes the form $\Phi_i \to (-1)^{i+1} \Phi_i$ $i = 1, 2$. Such a symmetry would also require $m_{12}^2 = 0$, unless we allow a soft violation of this discrete

symmetry by the dimension two term m_{12}^2. When this Z_2 symmetry is extended to the Yukawa sector we end up with four possibilities regarding the Higgs bosons couplings to the fermions. The two Z_2 symmetric models we will use in the work are the type II model—where the symmetry is extended in such a way that only Φ_1 couples to up-type quarks while only Φ_2 couples to down-type quarks and leptons—and the flipped model—where Φ_1 couples to up-type quarks and leptons while Φ_2 couples to the down-type quarks. Besides the type II and flipped scenarios, we will also study a version of the more general case of type III, to be discussed below, where neither the potential nor the Yukawa Lagrangian is Z_2 symmetric. Therefore, for this particular case, $\lambda_6 \neq 0$ and $\lambda_7 \neq 0$. Still in this work we will consider the limit $\lambda_6 \approx \lambda_7 \approx 0$. The reason is basically that of simplicity and it is justified by the fact that: (a) the study does not depend on those parameters as there are no Higgs self-coupling present in our analysis; (b) it is a tree-level study and $\lambda_6 \approx \lambda_7 \approx 0$ is a tree-level condition; (c) the only possible effect on our study would be to enlarge the allowed values of the parameter ranges which would not change our conclusions.

In the most general version of the 2HDM, the Yukawa sector is built such that both Higgs doublets couple to quarks and leptons. The model is known as 2HDM type III [27,28] and the Yukawa Lagrangian can be written as

$$
\begin{aligned}
-\mathcal{L}_Y = \bar{Q}_L (Y_1^d \Phi_1 + Y_2^d \Phi_2) d_R + \bar{Q}_L (Y_1^u \tilde{\Phi}_1 + Y_2^u \tilde{\Phi}_2) u_R \\
+ \bar{L}_L (Y_1^l \Phi_1 + Y_2^l \Phi_2) l_R + \text{H.c.},
\end{aligned}
$$

(4)

where $Q_L^T = (u_L, d_L)$ and $L_L^T = (l_L, l_L)$ are the left-handed quark doublet and lepton doublet, respectively, Y_k^f ($k = 1, 2$ and $f = u, d, l$) denote the 3×3 Yukawa matrices and $\tilde{\Phi}_k = i\sigma_2 \Phi_k^*$, $k = 1, 2$. Since the mass matrices of the quarks and leptons are a linear combination of Y_1^f and Y_2^f, $Y_{1,2}^{d,l}$ and $Y_{1,2}^u$ cannot be diagonalized simultaneously in general.[2] Therefore, neutral Higgs Yukawa couplings with flavor violation appear at tree-level and lead to a tree-level contribution to $\Delta M_{K,B,D}$ as well as to $B_{d,s} \to \mu^+ \mu^-$ mediated by neutral Higgs exchange. This is an important distinction with respect to Z_2 symmetric models and can have important repercussions for many different physical quantities. Note that also the charged Higgs coupling to a pair of fermions is modified, which will in turn induce changes in the contribution of the charged Higgs loop in $b \to s\gamma$ at the one-loop level. In order to get naturally small flavor changing neutral currents (FCNCs), we will use the Cheng-Sher ansatz by taking $Y_k^{i,j} \propto \sqrt{m_i m_j}/v$ [27,28].

---

[2]Since we are interested in the couplings of a charged Higgs boson to quarks we just consider that the lepton flavor violating couplings are small enough not to show any effect in the measured processes involving leptons.

TABLE I. Neutral Higgs Yukawa couplings in type II and type III relative to the SM Higgs Yukawa couplings with $\eta_{ij}^f = \sqrt{m_i/m_j}\chi_{ij}^f/v$. The Yukawa couplings for the flipped model are easily obtained from the type II ones with the replacements: $\xi_\Phi^{u,d,\ell}$ (flipped) = $\xi_\Phi^{u,d,u}$ (type II).

	ξ_Φ^u		ξ_Φ^d		ξ_Φ^ℓ	
Φ	Type II	Type III	Type II	Type III	Type II	Type III
h	$\frac{c_\alpha}{s_\beta}$	$\frac{c_\alpha}{s_\beta}\delta_{ij} - \eta_{ij}^f \frac{c_{\beta-\alpha}}{\sqrt{2}s_\beta}$	$-\frac{s_\alpha}{c_\beta}$	$-\frac{s_\alpha}{c_\beta}\delta_{ij} + \eta_{ij}^f \frac{c_{\beta-\alpha}}{\sqrt{2}c_\beta}$	$-\frac{s_\alpha}{c_\beta}$	$-\frac{s_\alpha}{c_\beta}\delta_{ij} + \eta_{ij}^f \frac{c_{\beta-\alpha}}{\sqrt{2}c_\beta}$
H	$\frac{s_\alpha}{s_\beta}$	$\frac{s_\alpha}{s_\beta}\delta_{ij} + \eta_{ij}^f \frac{s_{\beta-\alpha}}{\sqrt{2}s_\beta}$	$\frac{c_\alpha}{c_\beta}$	$\frac{c_\alpha}{c_\beta}\delta_{ij} - \eta_{ij}^f \frac{s_{\beta-\alpha}}{\sqrt{2}c_\beta}$	$\frac{c_\alpha}{c_\beta}$	$\frac{c_\alpha}{c_\beta}\delta_{ij} - \eta_{ij}^f \frac{s_{\beta-\alpha}}{\sqrt{2}c_\beta}$
A	$\frac{1}{t_\beta}$	$\frac{1}{t_\beta}\delta_{ij} - \eta_{ij}^f \frac{1}{\sqrt{2}s_\beta}$	t_β	$t_\beta\delta_{ij} - \eta_{ij}^f \frac{1}{\sqrt{2}c_\beta}$	t_β	$t_\beta\delta_{ij} - \eta_{ij}^f \frac{1}{\sqrt{2}c_\beta}$

After EWSB, the Yukawa Lagrangian can be expressed in the mass-eigenstate basis as [9,29]:

$$\mathcal{L}_Y = -\sum_{f=u,d,\ell} \frac{m_f}{v}(\xi_h^f \bar{f}fh + \xi_H^f \bar{f}fH - i\xi_A^f \bar{f}\gamma_5 fA)$$
$$-\left(\frac{\sqrt{2}V_{ud}}{v}\bar{u}(m_u\xi_A^u P_L + m_d\xi_A^d P_R)dH^+ + \text{H.c.}\right), \tag{5}$$

where the couplings ξ_Φ^f are given in Table I for type II, flipped, and type III. We stress that the parameters η_{ij}^f are related to the Yukawa couplings through the relations: $\eta_{ij}^u = U_L^u Y_1^u U_R^{u\dagger}/m_j$ and $\eta_{ij}^d = U_L^d Y_2^d U_R^{d\dagger}/m_j$, where $U_{L,R}^f$ are unitary matrices that diagonalize the fermions mass matrices. Using the Cheng-Sher ansatz, we assume that $\eta_{ij}^f = \sqrt{m_i/m_j}\chi_{ij}^f/v$ where χ_{ij}^f is a free parameter that will be taken in the range $[-1, 1]$. As can be seen from Table I, if the χ_{ij}^f's are of $\mathcal{O}(1)$, the new effects are dominated by heavy fermions and comparable with those in the 2HDM type II and flipped models. The effect of the χ_{ij}^f's can modify significantly the limit on the charged Higgs boson mass coming from $b \to s\gamma$. As recently discussed in [8], the mass of the charged Higgs boson is bounded to be heavier than about 580 GeV for any value of $\tan\beta$ in both the type II and flipped models. As shown in [9], though, this bound can be weakened to about 200 GeV by judiciously tuning the χ_{ij}^f's together with the other 2HDM type III parameters.

The couplings of h and H to gauge bosons $V = W, Z$ are proportional to $\sin(\beta - \alpha)$ and $\cos(\beta - \alpha)$, respectively. Since these are gauge couplings, they are the same for all Yukawa types. As we are considering the scenario where the neutral lightest Higgs state is the 125 GeV scalar, the SM-like Higgs boson h is recovered when $\cos(\beta - \alpha) \approx 0$. For the type II and flipped models, this is also the limit where the Yukawa couplings of the discovered Higgs boson become SM-like. The limit $\cos(\beta - \alpha) \approx 0$ seems to be favored by LHC data, except for the possibility of a wrong sign limit [30,31] where the couplings to down-type quarks can have a relative sign to the gauge bosons opposite to that of the SM. Our benchmarks will focus on the SM-like limit where indeed $\cos(\beta - \alpha) \approx 0$ and consequently the effect of the χ_{ij}^f's in $hf\bar{f}$ and $Hf\bar{f}$ coupling is suppressed by the $\cos(\beta - \alpha)$ factor.

III. THEORETICAL AND EXPERIMENTAL CONSTRAINTS

In order to perform a systematic scan on the versions of the 2HDM type II, flipped, and type III, we use the following theoretical and experimental constraints.

(i) *Vacuum stability*: To ensure that the scalar potential is bounded from below, the quartic couplings should satisfy the relations [32]

$$\lambda_{1,2} > 0, \qquad \lambda_3 > -(\lambda_1\lambda_2)^{1/2},$$
$$\text{and} \quad \lambda_3 + \lambda_4 - |\lambda_5| > -(\lambda_1\lambda_2)^{1/2}. \tag{6}$$

We impose that the potential has a minimum that is compatible with EWSB. If this minimum is CP-conserving, any other possible charged or CP-violating stationary points will be a saddle point above the minimum [33]. However, there is still the possibility of having two coexisting CP-conserving minima. In order to force the minimum compatible with EWSB, one can impose the simple condition [34]:

$$m_{12}^2(m_{11}^2 - m_{22}^2\sqrt{\lambda_1/\lambda_2})(\tan\beta - \sqrt[4]{\lambda_1/\lambda_2}) > 0. \tag{7}$$

Writing the minimum conditions as

$$m_{11}^2 + \frac{\lambda_1 v_1^2}{2} + \frac{\lambda_3 v_2^2}{2} = \frac{v_2}{v_1}\left[m_{12}^2 - (\lambda_4 + \lambda_5)\frac{v_1 v_2}{2}\right], \tag{8}$$

$$m_{22}^2 + \frac{\lambda_2 v_2^2}{2} + \frac{\lambda_3 v_1^2}{2} = \frac{v_1}{v_2}\left[m_{12}^2 - (\lambda_4 + \lambda_5)\frac{v_1 v_2}{2}\right] \tag{9}$$

allows us to express m_{11}^2 and m_{22}^2 in terms of the soft Z_2 breaking term m_{12}^2 and the quartic couplings λ_{1-5}.

(ii) *Perturbative unitarity*: Another important theoretical constraint on the scalar sector of 2HDMs stems from the perturbative unitarity requirement of the S-wave component of the various scalar scattering amplitudes. That condition implies a set of constraints that have to be fulfilled and are given by [35]

$$|a_\pm|, |b_\pm|, |c_\pm|, |f_\pm|, |e_{1,2}|, |f_1|, |p_1| < 8\pi, \quad (10)$$

where

$$a_\pm = \frac{3}{2}(\lambda_1 + \lambda_2) \pm \sqrt{\frac{9}{4}(\lambda_1 - \lambda_2)^2 + (2\lambda_3 + \lambda_4)^2},$$

$$b_\pm = \frac{1}{2}(\lambda_1 + \lambda_2) \pm \frac{1}{2}\sqrt{(\lambda_1 - \lambda_2)^2 + 4\lambda_4^2},$$

$$c_\pm = \frac{1}{2}(\lambda_1 + \lambda_2) \pm \frac{1}{2}\sqrt{(\lambda_1 - \lambda_2)^2 + 4\lambda_5^2},$$

$$e_1 = \lambda_3 + 2\lambda_4 - 3\lambda_5,$$

$$e_2 = \lambda_3 - \lambda_5,$$

$$f_+ = \lambda_3 + 2\lambda_4 + 3\lambda_5,$$

$$f_- = \lambda_3 + \lambda_5,$$

$$f_1 = \lambda_3 + \lambda_4,$$

$$p_1 = \lambda_3 - \lambda_4. \quad (11)$$

(iii) *EW precision tests*: The additional neutral and charged scalars contribute to the gauge boson vacuum polarization through their coupling to gauge bosons. As a result, the updated EW precision data provide important constraints on new physic models. In particular, the universal parameters S, T and U provides constraint on the mass splitting between the heavy states m_H, $m_{H^\pm}$ and m_A in the scenario in which h is identified with the SM-like Higgs state. The general expressions for the parameters S, T and U in 2HDMs can be found in [36]. To derive constraints on the scalar spectrum, we consider the following updated values for S, T and U:

$$\Delta S = 0.05 \pm 0.11, \qquad \Delta T = 0.09 \pm 0.13,$$

$$\Delta U = 0.01 \pm 0.11, \quad (12)$$

and use the corresponding covariance matrix given in [37]. The χ^2 function is then expressed as

$$\chi_{ST}^2 = \sum_{i,j}(X_i - X_i^{\text{SM}})(\sigma^2)_{ij}^{-1}(X_j - X_j^{\text{SM}}), \quad (13)$$

with correlation factor $+0.91$.

(iv) *LHC constraints*: Moreover, we take into account the new experimental data at 13 TeV from the observed cross section times branching ratio (BR) divided by the SM predictions, i.e., the so-called "signal strengths" of the Higgs boson defined by

$$\mu_i^f = \frac{\sigma(i \to h)^{\text{2HDM}}\text{BR}(h \to f)^{\text{2HDM}}}{\sigma(i \to h)^{\text{SM}}\text{BR}(h \to f)^{\text{SM}}}, \quad i = 1, 2,$$

$$(14)$$

where $\sigma(i \to h)$ denotes the Higgs boson production cross section through channel i and $\text{BR}(h \to f)$ the BR for the Higgs decay $h \to f$. Since several Higgs production channels are available at the LHC, they are grouped to be $\mu_1^f = \mu_{\text{ggF}+tth}^f$ and $\mu_2^f = \mu_{\text{VBF}+Vh}^f$, containing gluon-gluon Fusion (ggF) plus associated Higgs production $t\bar{t}h$ as well as Vector Boson Fusion (VBF) plus Higgs-strahlung Vh with $V = W^\pm, Z$. The values of the observed signal strengths are shown with their correlation factor in Table II. According to LHC results, which appear to be in good agreement with the SM predictions [38], the data seem to favor a scenario with alignment limit where $\sin(\beta - \alpha) \approx 1$ where h is the SM-like or $\cos(\beta - \alpha) \approx 1$ where H is the SM-like. As intimated, in our study, we identify the lightest CP-even state h with the SM-like scalar observed at the LHC with mass $m_h = 125.09(24)$ GeV [26] which, because we have discarded the possibility of being in the wrong sign limit, in turn implies that $\sin(\beta - \alpha) \approx 1$.

(v) *Flavor physics constraints*: We take into account all the relevant flavor constraints which, as previously discussed, force the charged Higgs mass to be above about 580 GeV from $b \to s\gamma$ at the 2σ level in type II and flipped [8]. However, we relax this condition to the 3σ level in order to obtain $H^\pm$ signal rates that are more within the reach of the next run of the LHC. All other flavor constraints were discussed recently for type III in [9] and are also taken into account here. We again note that the tuning of the χ_{ij}^f's together with the other 2HDM type III parameters allows us to relax the bound on the charged Higgs boson mass significantly in this scenario.

TABLE II. Combined best-fit signal strengths $\hat{\mu}_1$ and $\hat{\mu}_2$ for corresponding Higgs decay mode from [39].

f	$\hat{\mu}_1^f$	$\hat{\mu}_2^f$	$\pm 1\hat{\sigma}_1$	$\pm 1\hat{\sigma}_2$
$\gamma\gamma$	1.09	1.14	0.23	0.25
ZZ^*	1.31	1.25	0.24	0.28
WW^*	1.06	1.27	0.18	0.21
$\tau^+\tau^-$	1.05	1.24	0.35	0.40
$b\bar{b}$	3.9	3.7	2.8	2.4

IV. PARAMETER ESTIMATION AND BENCHMARKS

The above mentioned constraints are then imposed onto a set of randomly generated points in the ranges:

$$200 \text{ GeV} \leq m_{H^\pm} \leq 1 \text{ TeV},$$

$$126 \text{ GeV} \leq m_H \leq 1 \text{ TeV},$$

$$100 \text{ GeV} \leq m_A \leq 1 \text{ TeV},$$

$$-1 \leq \sin\alpha \leq 1,$$

$$2 \leq \tan\beta \leq 50,$$

$$-(1000 \text{ GeV})^2 \leq m_{12}^2 \leq (1000 \text{ GeV})^2. \quad (15)$$

We note again that we take the χ_{ij}^f's in the range $[-1, 1]$ and that all constraints are taken at the 2σ level except the ones from the $b \to s\gamma$ measurement where we allow

compatibility at the 3σ level which in type II and flipped mean a reduction in the bound from 580 to 440 GeV. For type III, the scan starts at 200 GeV.

In Fig. 1 (upper panels), we show the total widths of the CP-odd Higgs A and the charged Higgs boson $H^\pm$ in the plane $(m_A, m_{H^\pm})$. It is clear that the two widths can be simultaneously large. In the case of the charged Higgs boson, the total width is amplified by the opening of the bosonic decay $H^\pm \to W^\pm A$ for $m_A \leq 350$ GeV while for the CP-odd Higgs the total width gets enhanced after the opening of $A \to t\bar{t}$. In the lower panels of Fig. 1, we present the BRs of $A \to b\bar{b}$ (left) and $H^\pm \to W^\pm A$ (right). One can see that the BR$(A \to b\bar{b})$ could be sizeable and above about 70% below the $t\bar{t}$ threshold. In the case of the charged Higgs boson, since $g_{H^\pm W^\mp A}$ is a gauge coupling with no suppression factor, we expect BR$(H^\pm \to W^\pm A)$ to be large when kinematically allowed and able to compete with the $H^+ \to \bar{t}b$ and $H^\pm \to W^\pm H$ decays. The lighter the pseudoscalar is
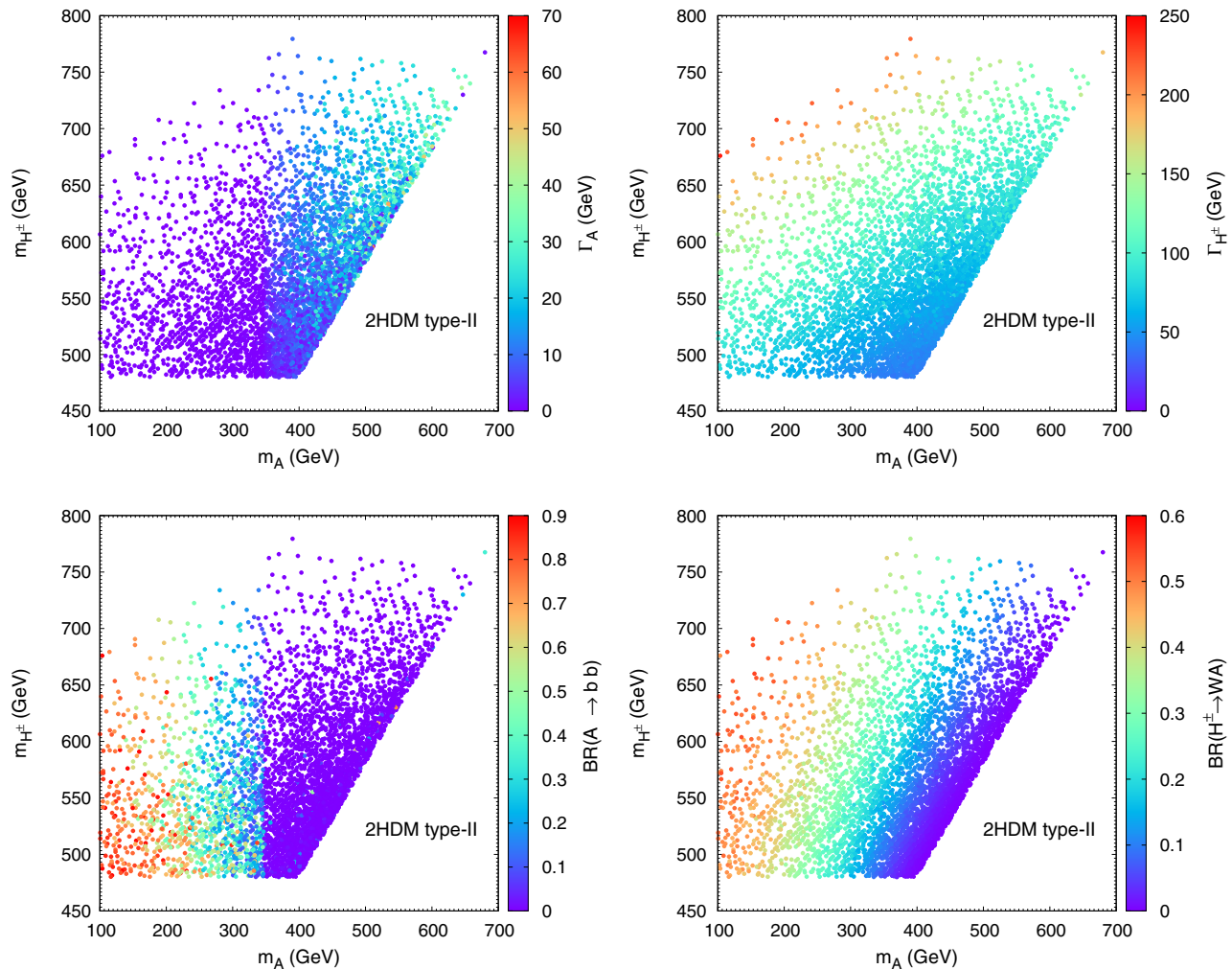

FIG. 1. Upper panels: Total decay widths (in GeV) of the CP-odd A and charged Higgs $H^\pm$ bosons in the plane $(m_A, m_{H^\pm})$. Lower panels: BR$(A \to b\bar{b})$ (left) and BR$(H^\pm \to W^\pm A)$ (right) in the plane $(m_A, m_{H^\pm})$. All panels are for type II.
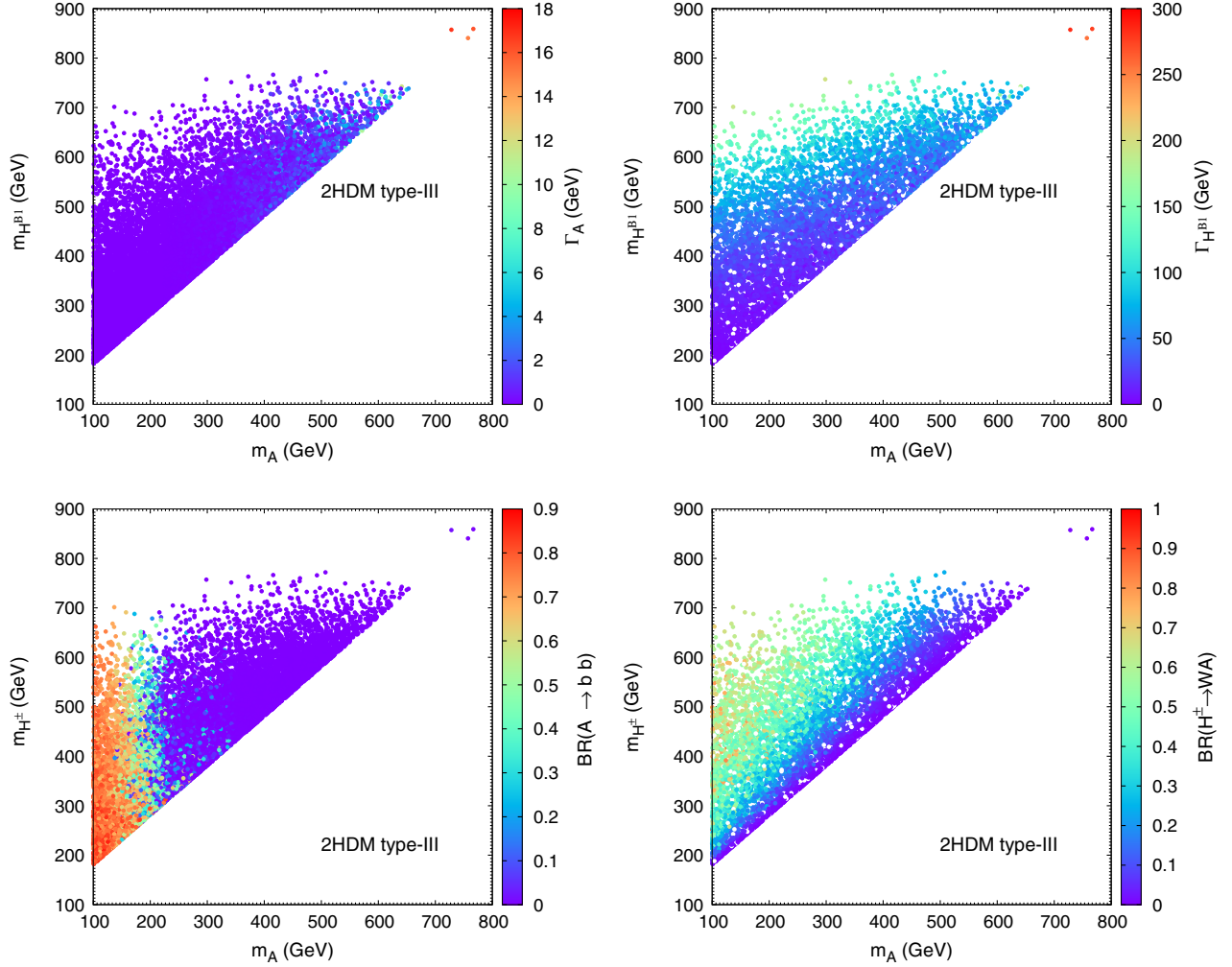
FIG. 2.   Same as in Fig. 1 but for type III.

the larger the BR($H^\pm \to W^\pm A$) can be, easily reaching values above 50% as can be seen from the figure. Therefore, since we need a charged Higgs boson with a large width, in order to compromise and to obtain large BR($H^\pm \to W^\pm A$) and large BR($A \to b\bar{b}$), we need a heavy charged Higgs and a much lighter pseudoscalar. Still the charged Higgs mass should not be too large so that the rate of signal events is large enough to be seen at the LHC Run II. We note that the plots for the flipped model would be very similar and therefore we will refrain from presenting them here.

In Fig. 2, we show the total width of the CP-odd A and of the charged Higgs boson $H^\pm$ together with BR($A \to b\bar{b}$) and BR($H^\pm \to W^\pm A$) in type III. The picture is rather similar to the one for type II except that the charged Higgs mass for type III is relaxed up to 200 GeV. The conclusions regarding the possible decays are the same as for type II and flipped.

V. MONTE CARLO SIMULATION AND RESULTS

We study the process $pp \to tW^-b\bar{b}$ wherein the interference effects between the charged Higgs resonant

diagrams (shown in Fig. 6 in the Appendix) and the nonresonant background graphs (presented in Figs. 7, 8, and 9, also in the Appendix) are found to be substantial. Nonresonant diagrams include all possible contributions coming from SM background as well as from 2HDM contributions. In total, there are 394 diagrams for the background contributing to the process $pp \to tW^-b\bar{b}$. The SM top-pair production associated with a b quark is the dominant component of the latter. We have calculated the interference effects between the resonant diagrams (from Fig. 6) and the diagrams which come from SM QCD interactions at the $\alpha_S^3 \alpha_{EW}$ order (Feynman diagrams with gluon contributions in Fig. 7 and diagrams 1–5 in Fig. 9) as well as with the ones that come from SM EW interactions at the $\alpha_S \alpha_{EW}^3$ order. We found that, in most cases, the EW contributions produce a small but positive interference with the signal while the QCD contributions a large negative one. Thus, the net result is generally an overall negative interference for the total cross section of the process $pp \to tW^-b\bar{b}$ and the magnitude of this interference is determined by the width of the intermediate

Higgs particles, i.e., A and $H^{\pm}$. However, for a minority of the benchmark points (BPs) to be studied, the overall effect can be positive.

As far as the signal is concerned, we focus on the dominant production mode of a heavy charged Higgs, i.e., $pp \to tH^{-}$, followed by its decay via $H^{-} \to W^{-}h \to W^{-}b\bar{b}$, $H^{-} \to W^{-}H \to W^{-}b\bar{b}$, $H^{-} \to W^{-}A \to W^{-}b\bar{b}$ and $H^{-} \to \bar{t}b \to W^{-}b\bar{b}$. Thus, all such decays lead to the same final state, facilitating interference effects amongst the different signal amplitudes. However, as previously shown in [23], interference effects amongst the signal contributions are generally negligible. Moreover, the BPs chosen in this study are such that the $H^{-} \to W^{-}A \to W^{-}b\bar{b}$ decay mode dominates over all other charged Higgs boson decays.

For the BPs of the models that we consider, we will focus on the mass of the scalars involved in the process, A and $H^{\pm}$, the BRs of the decays $H^{\pm} \to W^{\pm}A$ and $A \to b\bar{b}$ as well as the total width of the two scalars. As previously discussed, in order to have large interference effects between signal and background, the total width of the charged Higgs boson has to be quite large. However, to have a large interference, a sufficiently large width of the pseudoscalar is also essential. Otherwise, the decays of the A would be extremely narrow and would not overlap with any background processes. In this analysis, we first consider a 2HDM type II/flipped where the pseudoscalar couplings to down-type fermions are proportional to $\tan\beta$ so that, for a large values of it, the width of the pseudoscalar can be made significantly large. Taking into account the latest searches on $pp \to \Phi \to \tau^{+}\tau^{-}$ [40], Φ being any heavy spin-0 object, very large values of $\tan\beta$ are disallowed. In Table III, we present our input parameters for the type II and flipped models for five chosen BPs. The five points have passed all the constraints described before plus they are all valid for the flipped model as well since searches for $pp \to \Phi \to \tau^{+}\tau^{-}$ are negligible in the flipped case owing to the very small coupling to τ leptons for high $\tan\beta$. Therefore the five points are valid in the flipped model but only the first three are valid in type II. The latest searches for charged Higgs bosons by ATLAS [41,42] and CMS [43,44] are indeed in agreement with the values of the charged Higgs mass and the corresponding value of $\tan\beta$.

In Table IV, we present the partial widths for $\Gamma(A)$ and $\Gamma(H^{\pm})$ and the BR$(A \to b\bar{b})$, BR$(H^{+} \to b\bar{t})$ and

TABLE IV. Partial widths (in GeV) and BRs in type II and flipped for the BPs.

	$\Gamma(A)$	$\Gamma(H^{\pm})$	BR $(A \to b\bar{b})$	BR $(H^{+} \to b\bar{t})$	BR $(H^{+} \to W^{+}A)$
BP1 (II)	0.47	72.85	0.83	0.01	0.29
BP2 (II)	1.29	91.97	0.86	0.02	0.29
BP3 (II)	1.50	34.83	0.87	0.05	0.17
BP4 (F)	5.45	50.45	0.99	0.13	0.16
BP5 (F)	10.46	85.45	1.00	0.18	0.26

TABLE V. Cross sections (in pb) for signal, background, total and interference for the BPs of type II and flipped.

BP	Signal (pb)	Background (pb)	Total (pb)	Interference (pb)
BP1	0.031	10.03	9.96	−0.101
BP2	0.052	9.96	10.02	−0.008
BP3	0.144	10.07	10.18	0.034
BP4	0.469	9.94	10.31	−0.102
BP5	0.742	10.43	10.72	−0.452

BR$(H^{+} \to W^{+}A)$ for the five BPs. Note that the major difference between the models is the column for BR$(A \to b\bar{b})$ that is always larger in the flipped model because the decays to τ leptons become negligible in this model. For all other columns the differences are extremely small. This in turn means that the results are slightly better for the flipped model. We choose for the detailed analysis BP5 for of flipped model. Cross sections for signal, background, and total (including interference) for BP5 are 0.74, 10.43, and 10.72 pb, respectively. This results in an interference cross section of 0.45 pb which is around 60% of the signal cross section. The results for the cross sections for all BPs for the type II and flipped models are presented in Table V.

In the case of the type III model, we choose three BPs which are in agreement with all constraints. These are shown in Table VI and the corresponding widths and BRs are presented in Table VII.

For the type III, we choose the benchmark point BP2 which has the lightest $H^{\pm}$ mass and lowest mass splitting between $H^{\pm}$ and $W^{\pm}$ in order to demonstrate the interference effect in a wide range of mass spectra. For this benchmark point the cross sections for the signal, background and the total are 0.978 pb, 9.95 pb, and

TABLE III. Type II and flipped input parameters for the BPs.

	$\tan\beta$	$\sin(\beta-\alpha)$	$m_{H^{\pm}}$ (GeV)	m_{A} (GeV)	m_{12}^{2} (GeV^{2})
BP1 (II)	10.25	0.98	509.14	248.27	52 287.83
BP2 (II)	16.75	0.99	545.82	268.41	33 622.43
BP3 (II)	18.80	0.99	457.71	247.22	16 427.97
BP4 (F)	37.21	0.99	469.45	258.03	9 800.68
BP5 (F)	44.10	1.00	519.45	288.32	10 200.34

TABLE VI. Type III input parameters for the BPs.

	$\tan\beta$	$\sin(\beta-\alpha)$	$m_{H^{\pm}}$ (GeV)	m_{A} (GeV)	m_{12}^{2} (GeV^{-2})	χ
BP1	15.84	0.99	480.75	369.89	27 463.94	0.21
BP2	19.41	0.99	307.23	225.46	6 045.62	−0.34
BP3	38.11	0.99	447.45	258.33	9 833.68	0.71

TABLE VII.   Partial widths in units of GeV and BRs in type III.

	$\Gamma(A)$	$\Gamma(H^\pm)$	$BR(A \to b\bar{b})$	$BR(H^+ \to b\bar{t})$	$BR(H^+ \to W^+ A)$
BP1	2.79	60.72	0.47	0.02	0.27
BP2	1.69	12.78	0.88	0.05	0.21
BP3	6.10	52.77	0.87	0.10	0.17

TABLE VIII.   Cross sections (in pb) for signal, background, total and interference for the BPs in the 2HDM type III.

BP	Signal (pb)	Background (pb)	Total (pb)	Interference (pb)
BP1	0.059	10.35	10.27	−0.139
BP2	0.978	9.95	10.92	−0.008
BP3	0.291	10.02	10.34	0.029

10.92 pb, respectively. Thus, the resulting cross section turns out to be −0.008 pb. The small interference effect in this case can be attributed to the small width of both $H^\pm$ and A. The results for the cross sections for all BPs for the type III model are presented in Table VIII.

All the numbers presented above are at parton level. Next we perform a detector level analysis and study if these interference effects survive even after all acceptance and selection cuts. For this purpose, we generate the events using MadGraph [45] and then we pass these to Pythia [46] for parton showering and hadronization. Finally, we carried out a full detector simulation with DELPHES3 [47], which is a framework for the fast emulation of a generic collider experiment. For detector and trigger configurations, we resorted to the ATLAS default card. For b-tagging, we use the improved value of the efficiency from the ATLAS new b-tagging algorithm [48]. That is, in this analysis, we use a b-tagging efficiency according to following rule:

$$\epsilon_\eta \tanh(0.03 p_T - 0.4),$$

where $\epsilon_\eta = 0.7$ for $|\eta| \leq 1.2$ and 0.6 for $1.2 \leq |\eta| \leq 2.5$. We use this same expression for the probability of a c-jet faking a b-jet but now with $\epsilon_\eta = 0.2$ for $|\eta| \leq 1.2$ and $\epsilon_\eta = 0.1$ for $1.2 \leq |\eta| \leq 2.5$. Finally, for the light-quark and gluon jets, we take the mistagging probability to be 0.001 throughout.

Below we list the basic detector acceptance cuts.

(1) *Acceptance cuts*
  (a) Events must have at least one lepton (e or μ) and at least 5 jets.
  (b) Leptons must have transverse momentum $p_T > 20$ GeV and rapidity $|\eta| < 2.5$.
  (c) All jets must satisfy the following p_T and η requirements:

$$p_{Tj} > 20 \text{ GeV}, \qquad |\eta_j| < 2.5.$$

  (d) All pairs of objects must be well separated from each other,

$$\Delta R_{jj, jb, bb, \ell j, \ell b} \geq 0.4 \quad \text{where}$$
$$\Delta R = \sqrt{(\Delta \phi)^2 + (\Delta \eta)^2}.$$

A. Event reconstruction

In this section, we describe the procedure which we employ to reconstruct the masses of top quark, charged Higgs $H^\pm$, pseudoscalar A and the two $W^\pm$ bosons in each event. For this purpose, we make use of a method based on a χ^2 template [49]. We then discuss the efficiency of the reconstruction. Each event in the analysis is assumed to be a tH^- event decaying to $W^+ W^- jjj$ and one of the $W^\pm$ is considered to decay hadronically and the other leptonically. Thus, each single event is considered to have at least one lepton, five jets, and missing transverse energy.

The χ^2 fit takes as input the four vectors of the five leading jets, lepton and neutrino. The treatment of the neutrino four-vector is as follows. The transverse momentum of the neutrino is determine through balancing the initial and final particle momenta in an event. The longitudinal component of the neutrino momentum is instead determined by imposing the invariant mass constraint $M_{l\nu}^2 = M_{W^\pm}^2$. Since this condition leads to a quadratic equation, there are in general two solutions for p_ν^z:

$$p_\nu^z = \frac{1}{2 p_{\ell T}^2} \left(A_W p_\ell^z \pm E_\ell \sqrt{A_W^2 \pm 4 p_{\ell T}^2 E_{\nu T}^2} \right), \quad (16)$$

where $A_W = M_{W^\pm}^2 + 2 p_T \cdot E_{\nu T}$. A separate χ^2 is evaluated for each of the p_ν^z solutions and the one having minimum χ^2 value is retained to reconstruct the event.

We write two expressions for χ^2, one corresponding to a scenario where $H^\pm$ decays fully hadronically, χ_{had}^2, and other where it decays semileptonically, χ_{lep}^2:
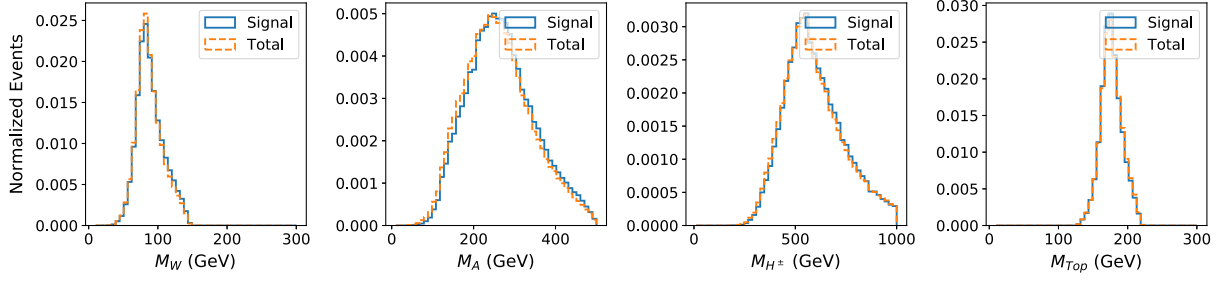
FIG. 3.   Reconstructed masses of $W^\pm$, pseudoscalar A, top quark and charged Higgs $H^\pm$ for BP5 in the 2HDM flipped.
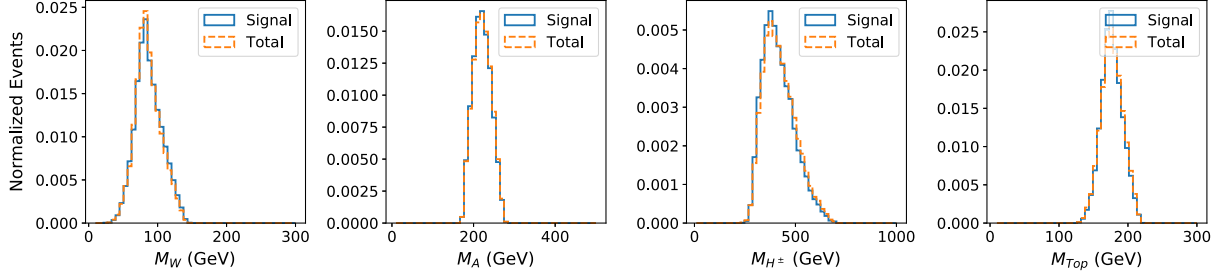
FIG. 4.   Reconstructed masses of $W^\pm$, pseudoscalar A, top quark and charged Higgs $H^\pm$ for BP2 in the 2HDM type III.

$$\chi^2_{\text{had}} = \frac{(M_{\ell\nu} - M_W)^2}{\Gamma^2_W} + \frac{(M_{jj} - M_W)^2}{\Gamma^2_W} + \frac{(M_{\ell\nu j} - M_{\text{top}})^2}{\Gamma^2_{\text{top}}} + \frac{(M_{jj} - M_A)^2}{\Gamma^2_A} + \frac{(M_{jjjj} - M_{H^\pm})^2}{\Gamma^2_{H^\pm}}, \tag{17}$$

$$\chi^2_{\text{lep}} = \frac{(M_{\ell\nu} - M_W)^2}{\Gamma^2_W} + \frac{(M_{jj} - M_W)^2}{\Gamma^2_W} + \frac{(M_{jjj} - M_{\text{top}})^2}{\Gamma^2_{\text{top}}} + \frac{(M_{jj} - M_A)^2}{\Gamma^2_A} + \frac{(M_{\ell\nu jj} - M_{H^\pm})^2}{\Gamma^2_{H^\pm}}, \tag{18}$$

where in the denominators we have the decay widths of the respective particles as calculated for the BPs in the various models.

For each event, χ^2 is evaluated for each possible way of assigning the five leading jets to the reconstructed top and charged Higgs four-momenta. The number of such permutations turns out to be 15 for each of χ^2_{had} and χ^2_{lep}. In addition, there is a twofold ambiguity in assigning the two solutions for p^z_ν. Finally, there are two ways with which two of the jets can be assigned to either a $W^\pm$ boson or to the pseudoscalar. Thus, for each event, the χ^2's are evaluated for 120 different combinations and the combination with minimum χ^2 values is kept for mass reconstruction.

Using the procedure described above, we now proceed to reconstruct the masses of the various particles involved in the process in order to see the efficiency of it. We present the reconstructed masses of all the intermediate resonant particles in the process, i.e., $W^\pm$, A, top and $H^\pm$ in Fig. 3 for the flipped case (BP5) and in Fig. 4 for the type III case (BP2). In each plot, we see that the peak is found to be at the particle masses, vouching for the effectiveness of our reconstruction procedure. In presenting the plots, we take events after applying all the acceptance cuts discussed above and selection cuts mentioned in Table IX.

In order to further investigate interference effects, we look at various distributions, e.g., transverse momentum

TABLE IX.   Cut flow of the cross sections for signal (BP5 in the 2HDM flipped) and irreducible background at the 14 TeV LHC. Conjugate processes are included here.

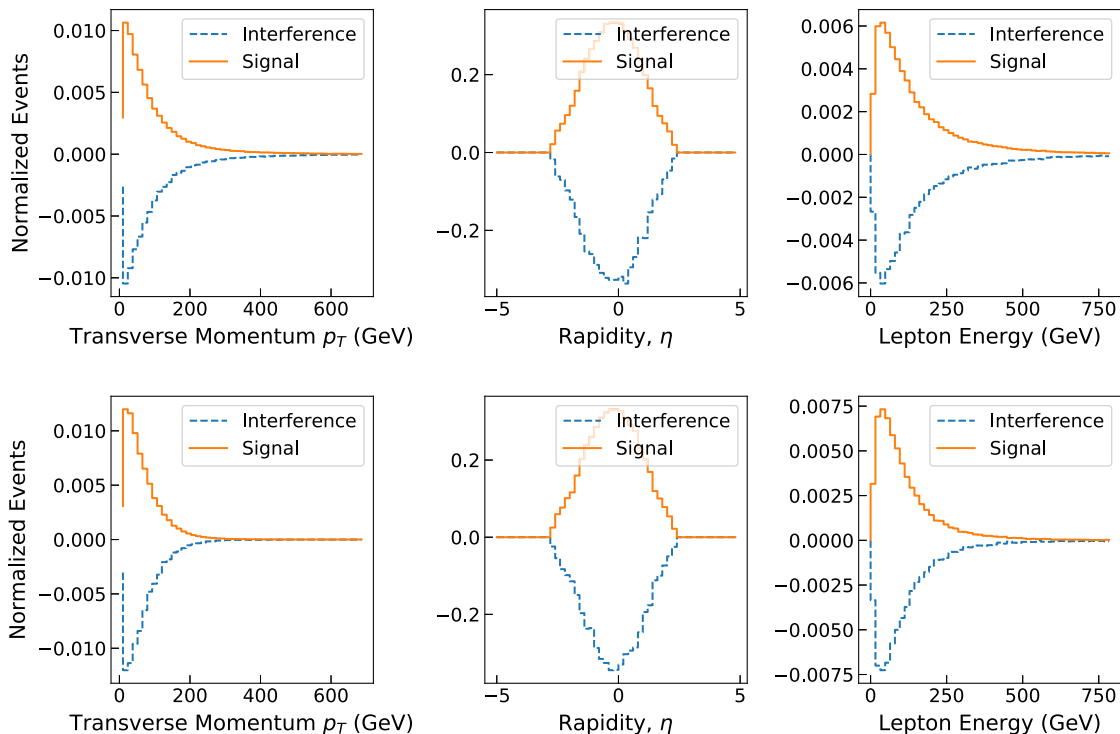|	σ [fb]			
Cuts	Signal	Background	Total	Interference
C0: No Cuts	740	10 430	10 720	−450
C1: Only one lepton	115.0	1 116.2	1 151.2	−80.1
C2: At least five light jets	91.9	680.8	703.5	−69.2
C3: Cut on $H_T > 500$ GeV	70.8	173.8	173.6	−71.1

FIG. 5. Distributions for transverse momentum, rapidity and energy of a lepton for signal and interference for BP5 of the 2HDM flipped (top) and BP2 of the 2HDM type III (bottom).

p_T, rapidity η and energy E of the lepton, for both the signal and interference contributions. The distributions for the interference are obtained by subtracting those of the signal and background processes (separately) from the total ones. The distributions for BP5 of the 2HDM flipped (top) and BP2 of the 2HDM type III (bottom) are shown in Fig. 5. We can clearly see that the shape of all distributions for signal alone and interference are almost the same but with opposite signs, the latter being expected, as we found the overall interference between signal and irreducible background to be destructive for the used BP. It is instead remarkable the similarity found between the two contributors to the total signal cross section. Notice that in Fig. 5 we have only shown the

lepton distributions though it has been verified for all the jets involved in the process that their distributions present the same behavior.

Finally, we present in Table IX the flow of cross section values after each cut for (flipped) BP5 and in Table X for (type III) BP2. We observe that the relative ratio of the signal-to-interference cross section increases with each cut for both BPs. For (flipped) BP5, we see that the ratio rises from 60% to almost larger than 100% while, for (type III) BP2, the increment is from 0.1% to 17%. The reason for the smaller interference cross section for the latter with respect to the former is a smaller width for both A and $H^{\pm}$: this well illustrates the correlation between interference effects and off-shellness of the Higgs bosons involved.

TABLE X. Cut flow of the cross sections for signal (BP2 in the 2HDM type III) and irreducible background at the 14 TeV LHC. Conjugate processes are included here.

	σ [fb]			
Cuts	Signal	Background	Total	Interference
C0: No Cuts	978	9 950	10 920	−8
C1: Only one lepton	243.6	2 040.8	1 151.2	−6.4
C2: At least five light jets	180.3	1 221.4	1 398.1	−3.6
C3: Cut on $H_T > 500$ GeV	89.8	491.2	566.9	−14.1

VI. CONCLUSIONS

In this paper, we have assessed whether interference effects involving heavy charged Higgs signals appearing via $W^{\pm}b\bar{b}$ final states at the LHC, both amongst themselves and in relation to irreducible background, can be sizable and thus affect ongoing experimental searches. We have taken as reference models to perform our analysis two Z_2 symmetric 2HDMs, the type II and flipped versions, as well as the type III one. We have then prepared the corresponding parameter space regions amenable to phenomenological investigation by enforcing both theoretical (i.e., unitarity, perturbativity, vacuum stability, triviality) and experimental (i.e., from flavor physics, void and successful Higgs boson searches at the Tevatron and LHC, EW precisions observables from LEP and SLC) constraints. We have finally proceeded to simulate the relevant signal processes via $bg \to tH^-$ (+c.c.) scattering with the charged Higgs state decaying via $H^- \to W^- h, A, H \to W^- b\bar{b}$ or $H^- \to \bar{t}b \to W^- b\bar{b}$ (+c.c. in all cases) and the irreducible background given by $bg \to tW^- b\bar{b}$ topologies. The motivation for this is that signals and background are treated separately in current approaches. Indeed, these may be invalidated by the fact that, on the one hand, a heavy charged Higgs state can have a large width and, on the other hand, this can also happen for (some of) the neutral Higgs states emerging from its decays. Clearly, a prerequisite for such interference effects to onset is that such widths are large enough, say, 10% or so, which we have verified here to be the case. While the phenomenology we have investigated could well occur in the other decay chains in suitable regions of the parameter space, we have chosen to single out here $H^- \to W^- A \to W^- b\bar{b}$, as it is the one that is most subject to interference effects with the irreducible background, at least in the 2HDM type II, flipped, and type III setups adopted. In fact, the latter are generally predominant over interference effects amongst the different decay patterns of the $H^{\pm}$ signal.

After performing a sophisticated MC simulation, we have seen that such interference effects can be very large, even of $\mathcal{O}(100\%)$, both before and after $H^{\pm}$ selection cuts are enforced, and mostly negative. This appears to be the case for all masses tested, from 300 to 500 GeV or so, in both the 2HDM II and flipped as well as type III, the more so the larger the $H^{\pm}$ and A masses (and, consequently, their widths). Remarkably, after all cuts are applied, the shapes of the analyzed signal and interference (with the irreducible background) are essentially identical in all kinematical observables relevant to the signal extraction, as the selection drives these two components of the total cross section to be very similar. These findings therefore imply that current and, especially, future LHC sensitivities to heavy charged Higgs bosons signals in $W^- b\bar{b}$ final states require an "inclusive" rescaling of the event yields, as the 'exclusive' shape of the signal is roughly unchanged after such interference effects are accounted for.

APPENDIX: REPRESENTATIVE FEYNMAN DIAGRAMS FOR $pp \rightarrow tW^-b\bar{b}$

In this appendix, we present the Feynman diagrams for the process $pp \rightarrow tW^-b\bar{b}$. The resonant diagrams are depicted in Fig. 6 and the nonresonant background graphs are shown in Figs. 7, 8, and 9.
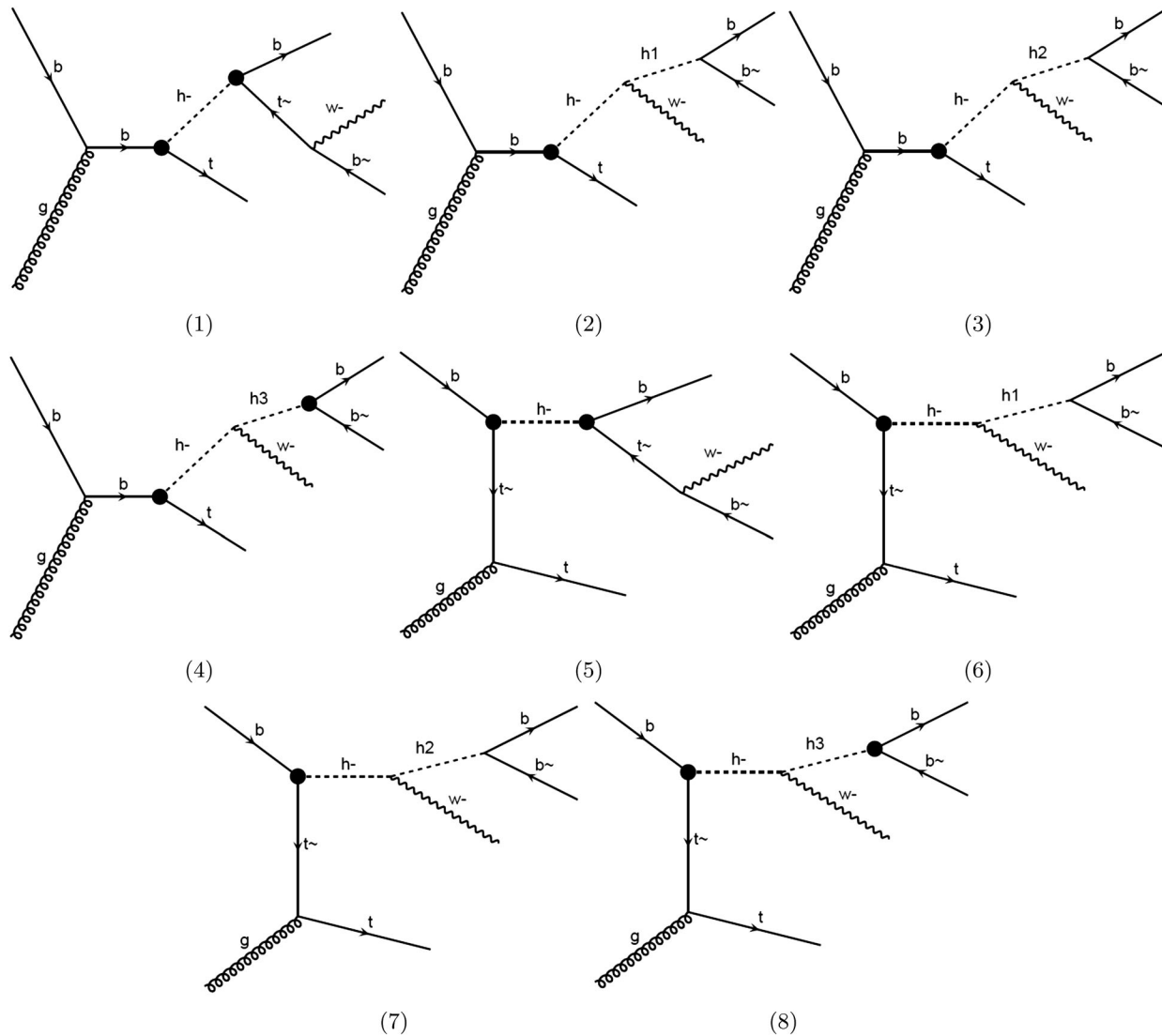

FIG. 6.   Feynman diagrams in a 2HDM contributing to resonant charged Higgs production and corresponding decays leading to the signal $pp \rightarrow tW^-b\bar{b}$ with h- $\equiv H^-$, h1 $\equiv h$, h2 $\equiv H$, and h3 $\equiv A$ (as appropriate).
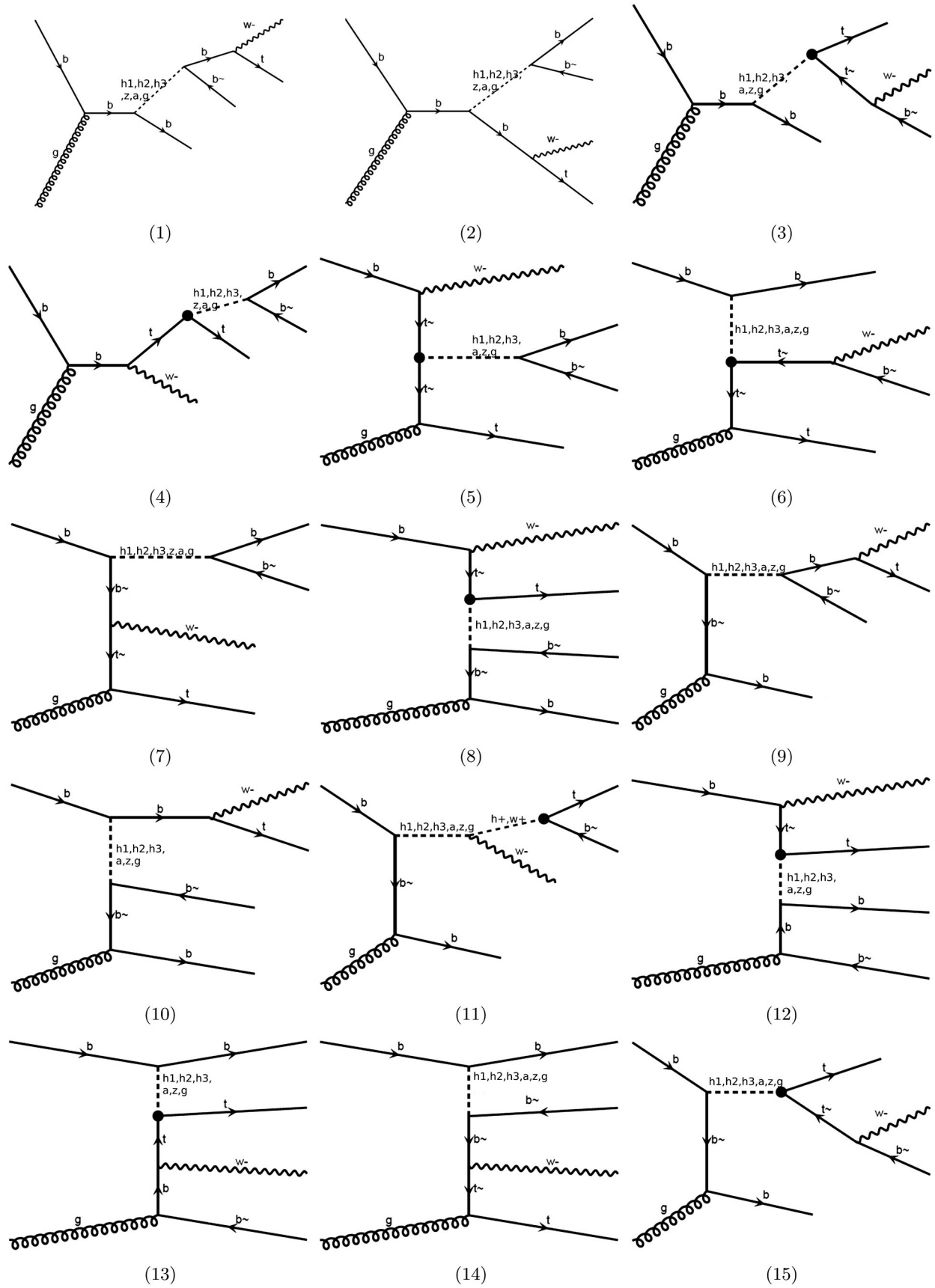
FIG. 7. Nonresonant Feynman diagrams contributing to the background for the process $pp \to tW^- b\bar{b}$ with h- $\equiv H^-$, h1 $\equiv h$, h2 $\equiv H$, h3 $\equiv A$, and a $\equiv \gamma$ (as appropriate).
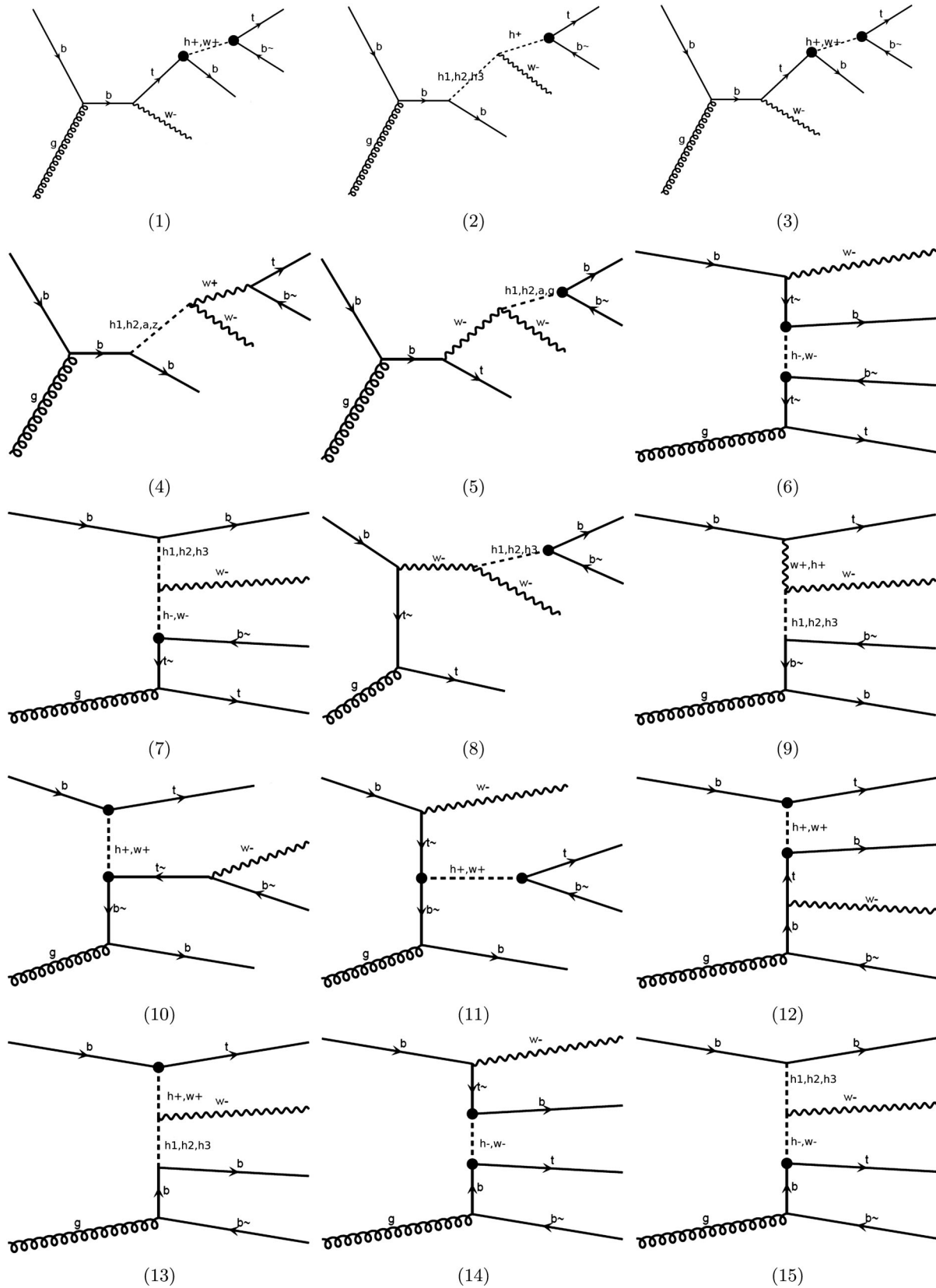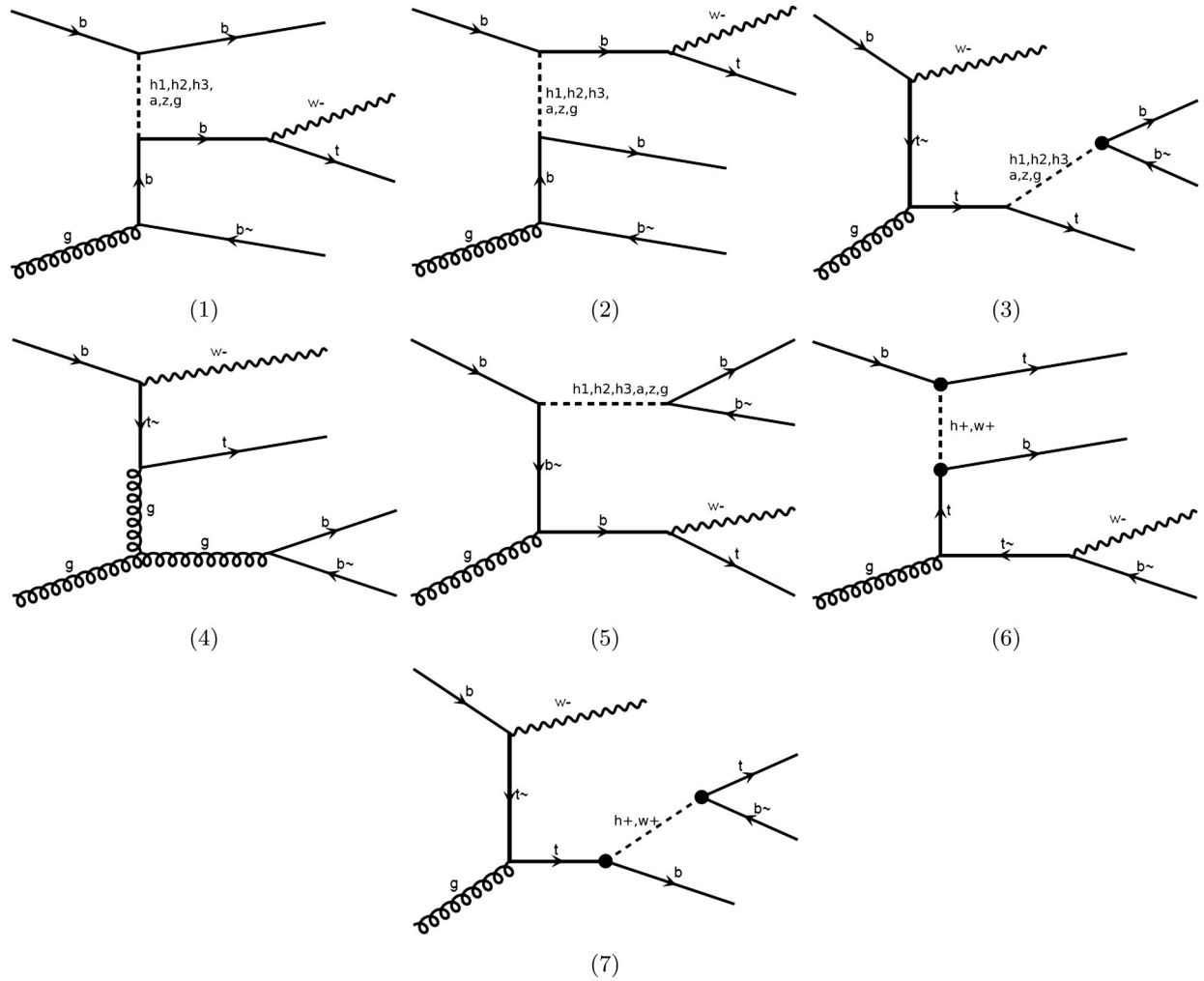
FIG. 8.   Nonresonant Feynman diagrams contributing to the background for the process $pp \rightarrow tW^- b\bar{b}$ with h- $\equiv H^-$, h1 $\equiv h$, h2 $\equiv H$, h3 $\equiv A$, and a $\equiv \gamma$ (as appropriate).

FIG. 9.   Nonresonant Feynman diagrams contributing to the background for the process $pp \to tW^-b\bar{b}$ with h- $\equiv H^-$, h1 $\equiv h$, h2 $\equiv H$, h3 $\equiv A$, and a $\equiv \gamma$ (as appropriate).

[1] M. Aoki, R. Guedes, S. Kanemura, S. Moretti, R. Santos, and K. Yagyu, Phys. Rev. D **84**, 055028 (2011).

[2] G. Arnison *et al.* (UA1 Collaboration), Phys. Lett. **122B**, 103 (1983).

[3] P. Bagnaia *et al.* (UA2 Collaboration), Phys. Lett. **129B**, 130 (1983).

[4] G. Aad *et al.* (ATLAS Collaboration), Phys. Lett. B **716**, 1 (2012).

[5] S. Chatrchyan *et al.* (CMS Collaboration), Phys. Lett. B **716**, 30 (2012).

[6] G. C. Branco, P. M. Ferreira, L. Lavoura, M. N. Rebelo, M. Sher, and J. P. Silva, Phys. Rep. **516**, 1 (2012); I. P. Ivanov, Prog. Part. Nucl. Phys. **95**, 160 (2017).

[7] M. Misiak *et al.*, Phys. Rev. Lett. **114**, 221801 (2015).

[8] M. Misiak and M. Steinhauser, Eur. Phys. J. C **77**, 201 (2017).

[9] A. Arhrib, R. Benbrik, C. H. Chen, J. K. Parry, L. Rahili, S. Semlali, and Q. S. Yan, arXiv:1710.05898.

[10] J. F. Gunion, H. E. Haber, F. E. Paige, W. K. Tung, and S. S. D. Willenbrock, Nucl. Phys. **B294**, 621 (1987).

[11] S. Moretti and K. Odagiri, Phys. Rev. D **55**, 5627 (1997).

[12] A. A. B. Bendezu and B. A. Kniehl, Phys. Rev. D **59**, 015009 (1998).

[13] S. Moretti and K. Odagiri, Phys. Rev. D **59**, 055008 (1999).

[14] V. D. Barger, R. J. N. Phillips, and D. P. Roy, Phys. Lett. B **324**, 236 (1994).

[15] J. F. Gunion, Phys. Lett. B **322**, 125 (1994).

[16] D. J. Miller, S. Moretti, D. P. Roy, and W. J. Stirling, Phys. Rev. D **61**, 055011 (2000).

[17] S. Moretti and D. P. Roy, Phys. Lett. B **470**, 209 (1999).

[18] G. Aad *et al.* (ATLAS Collaboration), J. High Energy Phys. 03 (2016) 127.

[19] V. Khachatryan *et al.* (CMS Collaboration), J. High Energy Phys. 11 (2015) 018.

[20] R. Enberg, W. Klemm, S. Moretti, S. Munir, and G. Wouda, Nucl. Phys. **B893**, 420 (2015).

[21] M. Drees, M. Guchait, and D. P. Roy, Phys. Lett. B **471**, 39 (1999).

[22] S. Moretti, Phys. Lett. B **481**, 49 (2000).

[23] S. Moretti, R. Santos, and P. Sharma, Phys. Lett. B **760**, 697 (2016).

[24] A. G. Akeroyd *et al.*, Eur. Phys. J. C **77**, 276 (2017).

[25] J. F. Gunion and H. E. Haber, Phys. Rev. D **67**, 075019 (2003).

[26] C. Patrignani *et al.* (Particle Data Group Collaboration), Chin. Phys. C **40**, 100001 (2016).

[27] T. P. Cheng and M. Sher, Phys. Rev. D **35** (1987) 3484.

[28] D. Atwood, L. Reina, and A. Soni, Phys. Rev. D **55**, 3156 (1997); C.-H. Chen and C.-Q. Geng, Phys. Rev. D **71**, 115004 (2005).

[29] M. Gomez-Bock and R. Noriega-Papaqui, J. Phys. G **32**, 761 (2006); M. Gomez-Bock, G. L. Castro, L. Lopez-Lozano, and A. Rosado, Phys. Rev. D **80**, 055017 (2009).

[30] P. M. Ferreira, J. F. Gunion, H. E. Haber, and R. Santos, Phys. Rev. D **89**, 115003 (2014).

[31] P. M. Ferreira, R. Guedes, M. O. P. Sampaio, and R. Santos, J. High Energy Phys. 12 (2014) 067.

[32] N. G. Deshpande and E. Ma, Phys. Rev. D **18**, 2574 (1978).

[33] P. M. Ferreira, R. Santos, and A. Barroso, Phys. Lett. B **603**, 219 (2004); **629**, 114(E) (2005).

[34] A. Barroso, P. M. Ferreira, I. P. Ivanov, and R. Santos, J. High Energy Phys. 06 (2013) 045.

[35] A. G. Akeroyd, A. Arhrib, and E. M. Naimi, Phys. Lett. B **490**, 119 (2000); A. Arhrib, arXiv:hep-ph/0012353.

[36] R. Barbieri, L. J. Hall, Y. Nomura, and V. S. Rychkov, Phys. Rev. D **75**, 035007 (2007).

[37] M. Baak *et al.* (Gfitter Group Collaboration), Eur. Phys. J. C **74**, 3046 (2014).

[38] T. Corbett, O. J. P. Eboli, D. Goncalves, J. Gonzalez-Fraile, T. Plehn, and M. Rauch, J. High Energy Phys. 08 (2015) 156.

[39] ATLAS Collaboration, ATLAS-CONF-2016-081; ATLAS Collaboration, ATLAS-CONF-2016-063; ATLAS Collaboration, ATLAS-CONF-2016-003; CMS Collaboration, CMS-PAS-HIG-16-020; CMS Collaboration, CMS-PAS-HIG-16-038.

[40] M. Aaboud *et al.* (ATLAS Collaboration), J. High Energy Phys. 01 (2018) 055; CMS Collaboration, Report No. CMS-PAS-HIG-17-020.

[41] G. Aad *et al.* (ATLAS Collaboration), J. High Enery Phys. 03 (**2016**) 127.

[42] M. Aaboud *et al.* (ATLAS Collaboration), Phys. Lett. B **759**, 555 (2016).

[43] V. Khachatryan *et al.* (CMS Collaboration), J. High Energy Phys. 11 (2015) 018.

[44] CMS Collaboration, Report No. CMS-PAS-HIG-16-027.

[45] J. Alwall, R. Frederix, S. Frixione, V. Hirschi, F. Maltoni, O. Mattelaer, H.-S. Shao, T. Stelzer, P. Torrielli, and M. Zaro, J. High Energy Phys. 07 (2014) 079.

[46] T. Sjöstrand, S. Ask, J. R. Christiansen, R. Corke, N. Desai, P. Ilten, S. Mrenna, S. Prestel, C. O. Rasmussen, and P. Z. Skands, Comput. Phys. Commun. **191**, 159 (2015).

[47] S. Ovyn, X. Rouby, and V. Lemaitre, arXiv:0903.2225.

[48] ATLAS Collaboration, Report No. ATL-PHYS-PUB-2015-022.

[49] E. L. Berger, Q. H. Cao, J. H. Yu, and C.-P. Yuan, Phys. Rev. D **84**, 095026 (2011).